Porphyry Vectoring within Advanced Argillic-Altered Rocks of British Columbia

F. Bouzari, Mineral Deposit Research Unit, The University of British Columbia, Vancouver, British Columbia, fbouzari@eoas.ubc.ca

R.G. Lee, Mineral Deposit Research Unit, The University of British Columbia, Vancouver, British Columbia

C.J.R. Hart, Mineral Deposit Research Unit, The University of British Columbia, Vancouver, British Columbia

B.I. van Straaten, British Columbia Geological Survey, Victoria, British Columbia

Bouzari, F., Lee, R.G., Hart, C.J.R. and van Straaten, B.I. (2020): Porphyry vectoring within advanced argillic-altered rocks of British Columbia; *in* Geoscience BC Summary of Activities 2019: Minerals, Geoscience BC, Report 2020-01, p. 115–130.

Introduction

Porphyry copper deposits commonly form vertical bodies of mineralized rock and alteration zones that vary depending on depth, fluid composition and hostrock. In many calcalkalic-type porphyry deposits, a large blanket of advanced argillic-altered rocks that are characterized by abundant quartz and clay minerals form a cap above the main porphyry intrusion. However, the location of the porphyry system beneath this lithocap is rarely apparent and new tools are required to inform exploration decision-making in these geological situations.

The application of alteration studies has played a key role in the discovery of several porphyry deposits, and recent research at The University of British Columbia's Mineral Deposit Research Unit (MDRU) has identified the distal alteration-footprint characteristics of the porphyry system (e.g., Halley et al., 2015; Lesher et al., 2017), and the use of resistate minerals for alteration studies (e.g., Bouzari et al., 2016). However, most of these studies focused on the broader alteration footprints of the porphyry system and did not examine the advanced argillic alteration above these systems.

Advanced argillic alteration has been preserved at several British Columbia (BC) localities (Table 1). Studies in the Toodoggone district (Bouzari et al., 2019), the Bonanza volcanic field in northern Vancouver Island (Panteleyev and Koyanagi, 1994), Limonite Creek in central BC (Deyell et al., 2000) and several other locations in BC have recognized linkages to porphyry-type mineralization at depth. Identifying the textural, mineralogical and geochemical trends within these advanced argillic-alteration zones will guide BC explorers in better identifying porphyry copper potential and provide tools that point toward mineralization.

Table 1. Localities with advanced argillic alteration in British Columbia (after Panteleyev, 1992).

Property	Advanced argillic alteration	High-sulphidation-type sulphide	Porphyry-type alteration or veins
Sutlahine River area:			
Thorn, Daisy, Ink, Camp Creek	X	X	X
Kay, Lin, Lin 1-8	X	X	
Iskut River Area:			
Johnny Mountain/REG/Quartz Rise	X	X	
Treaty Glacier	X		
Dease Lake area:			
Tanzilla-McBride	X		X
Toodoggone River area:			
Alunite Ridge	X	X	X
Quartz Lake	X		
Brenda	X	X	
Black Gossan	X		X
Silver Pond	X		
Baker	X		X
Central BC:			
Equity Silver mine	X		
Limonite Creek	X		X
Taseko River/Mount McClure area:			
Empress	X		
Taylor-Windfall	X	X	
Vancouver Island:			
Hushamu	X	X	X
Macintosh, Pemberton Hills	X		
Red Dog	X		
Wanokana	X		
Island Copper mine	X		X
Kyuquot Sound (Easy Inlet)	X		
Southern BC:			
Riverside	X		
Pyro	X		

This publication is also available, free of charge, as colour digital files in Adobe Acrobat® PDF format from the Geoscience BC website: http://www.geosciencebc.com/updates/summary-of-activities/.

Tops of Porphyry Systems

Advanced argillic alteration in upper parts of porphyry copper systems are known as 'lithocaps' because they cap porphyry deposits, have a blanket-like geometry with areal extents of >10 km^2 and reach a thickness of up to 1 km. Therefore, advanced argillic-alteration zones can form the largest near-surface footprint of porphyry copper systems. Indeed, two or more porphyry copper deposits may underlie some large, coalesced advanced argillic zones (Sillitoe, 2010) and advanced argillic-alteration zones themselves may host high-sulphidation epithermal-type gold mineralization in those locations where they are preserved from erosion.

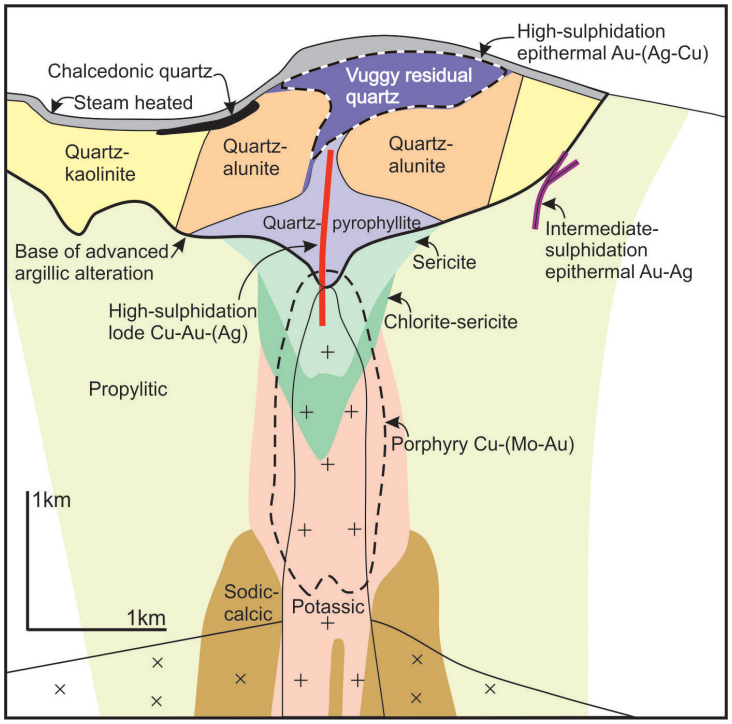

Figure 1. Schematic cross-section showing the main components of advanced argillic alteration above a zone of porphyry mineralization in the study area (after Sillitoe, 2010).

The advanced argillic zones tend to be vertically zoned, from quartz-pyrophyllite locally with andalusite and diaspore at depth to predominantly quartz-alunite and residual quartz with a vuggy appearance at shallower levels. Laterally, kaolinite predominates with topaz and zunyite, and locally fluorite in F-rich systems (Figure 1). In the shallowest zones that form within the paleo–water table, subhorizontal, tabular bodies of massive opaline or chalcedonic silicification, up to 10 m or so thick, are deposited, while steam-heated alteration is characterized by fine-grained, powdery cristobalite, alunite and kaolinite in the overlying vadose zones (Sillitoe, 1993, 2000).

The development of advanced argillic alteration is attributed to two hydrothermal stages (e.g., Simmons et al., 2005):

1) an early stage of intense acid leaching of the wallrocks, which results from magmatic vapours that cool to <300 °C and condense into groundwaters that are acidified by dissociation of potent acids such as HCl or H_2SO_4 (Hedenquist and Taran, 2013)
2) a second stage, which develops from weakly acidic fluid that deposits the bulk of the sulphide minerals and precious metals with euhedral quartz precipitate (Stoffregen, 1987; Heinrich et al., 2004; Heinrich, 2007)

Vectoring in Advanced Argillic Alteration

The recognition of mineralogical patterns within areas of advanced argillic alteration provides a fundamental opportunity to identify the presence of high-sulphidation epithermal-gold and potential underlying porphyry mineralization. Minerals such as diaspore and andalusite with pyrophyllite occur at the roots of advanced argillic alteration above the porphyry system, whereas zones of residual quartz, quartz-alunite and quartz-kaolinite occur laterally in more permeable hostrocks at higher levels.

Mineral exploration in advanced argillic zones is traditionally difficult for several reasons. These alteration zones can cover large areas (>10 km) and not only are the mineralogical changes cryptic but they could be affected by the hostrock composition or obliterated by subsequent supergene weathering effects. Advanced argillic alteration is well developed in hostrocks with low acid-buffering capacity, whereas rocks with high acid-buffering capacity produce weaker advanced argillic alteration and may not develop the typical mineral zoning. As a result, alunite may not form in some areas. Alunite composition itself has been used as a vector toward mineralization (e.g., Chang et al., 2011), but other studies (e.g., Deyell and Dipple, 2005) have shown that alunite chemistry is influenced by hostrocks, may vary between fluid pulses and does not necessarily reflect proximity to mineralization. Moreover, in these environments, alunite can form in at least three types of zones: 1) in the high-sulphidation alteration zone above the pyrophyllite zone; 2) in the steam-heated alteration zone near the surface; and 3) within the overprinting supergene alteration zone. Therefore, distinguishing each of the alunite types, using techniques such as texture and composition, is of significant importance in exploration.

The most abundant mineral within advanced argillic-alteration zones is quartz. Most quartz is residual after intense acid leaching and has a vuggy texture; it can also occur with low-pH stable alunite or kaolinite. Quartz can form during the early barren alteration phase and can be deposited dur-

ing the later gold-mineralization stages. Textures and cathodoluminescence characteristics of the quartz have been used to identify the ore-stage quartz (T. Bissig, pers. comm., 2016).

Clay minerals, such as illite, kaolinite, dickite and montmorillonite are widespread in advanced argillic alteration. The distribution of clay minerals and, more importantly, their crystallinity are useful tools to use as vectors toward rocks affected by higher temperature alteration. However, advanced argillic-alteration zones typically contain abundant, fine-grained disseminated pyrite. Oxidation of pyrite during the supergene processes also generates acids and abundant clays (mostly kaolinite), and can obliterate the hypogene mineralogy. Therefore, distinction of supergene clay and identifying the remnants of hypogene advanced argillic alteration is important in areas affected by supergene oxidation.

Geological Setting

Advanced argillic-alteration zones occur in several locations in BC, commonly within the districts that are highly prospective to host porphyry-type copper mineralization (Table 1). They occur throughout BC but cover larger areas in northern BC and Vancouver Island. Some of these areas have been evaluated to host epithermal-type gold mineralization, but evidence for underlying porphyry-type copper mineralization has been shown to occur in several locations such as in the Toodoggone and Sutlahine River areas and on Vancouver Island (Table 1). Moreover, these highly-altered areas could also be considered to have resource potential for kaolinite and silica (Shearer et al., 2004).

In this study, three areas in northern BC with notable advanced argillic-alteration zones are evaluated: Tanzilla, Alunite Ridge and Kemess North (Figure 2).

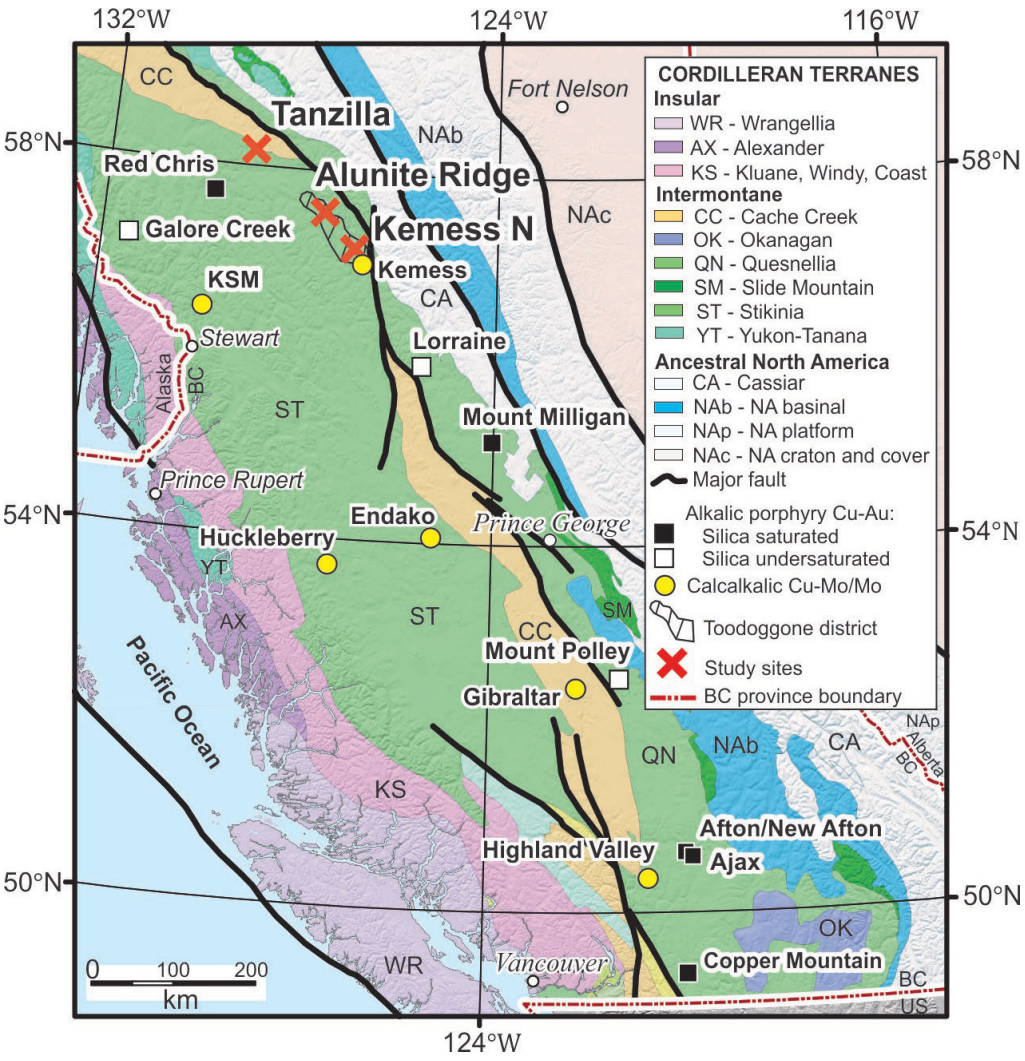

Figure 2. Cordilleran terranes of British Columbia showing the location of the study areas (after Bissig and Cooke, 2014).

Tanzilla

The Tanzilla property is within the Intermontane belt, near the northeastern margin of the Stikine terrane (Figure 2), a Late Triassic–Early Jurassic volcanic island-arc complex that was accreted to ancestral North America during the Middle Jurassic (Nelson and Mihalynuk, 1993). The property is underlain by a volcanic succession about 4.5 km thick assigned to the Horn Mountain Formation (late Early to Middle Jurassic; van Straaten and Nelson, 2016) in the upper part of the Hazelton Group (Figure 3). The lower part of the Horn Mountain Formation includes massive green augite-plagioclase-phyric volcanic breccia (not exposed in the study area), whereas the middle part is mainly maroon volcanic breccias, autobreccias and flows, and includes minor laminated felsic tuffs to bedded lapillistone. The upper parts of the Horn Mountain Formation consist of a felsic volcanic unit of mainly aphanitic and plagioclase-phyric clasts capped by a mafic volcanic unit of augite-plagioclase–phyric volcanic breccias and flows (van Straaten and Gibson, 2017). These units are unconformably overlain by sedimentary rocks of the Bowser Lake Group. To the north, folded Takwahoni Formation siliciclastic rocks (Early Jurassic) deposited in the Whitehorse trough are in the hangingwall of the Kehlechoa thrust fault. The Late Jurassic Snowdrift Creek pluton (160.43 ±0.16 Ma; van Straaten and Gibson, 2017) cuts the Horn Mountain strata and the Kehlechoa thrust fault. Moderate to intense pervasive biotite alteration is reported from several hundred metres up to one kilometre from the margin of the Snowdrift Creek pluton (van Straaten and Gibson, 2017).

The Horn Mountain Formation hosts areally extensive advanced argillic alteration at the Tanzilla-McBride property for at least 17 km along strike (van Straaten and Gibson, 2017; van Straaten and Bouzari, 2018). At Tanzilla, the advanced argillic-alteration zone is at least 5 by 2 km and overlies porphyry-style alteration at depth, which is characterized by quartz-sericite-pyrite to potassic alteration with anomalous copper and molybdenum centred around a 173 Ma plagioclase porphyry body (van Straaten and Nelson, 2016; van Straaten and Gibson, 2017).

Recent work at Tanzilla includes geophysical surveys, diamond drilling, mapping and a shortwave-infrared (SWIR) alteration-mineral study (Luckman et al., 2013; Barresi et al., 2014; van Straaten and Gibson, 2017; van Straaten and Bouzari, 2018).

Alunite Ridge

Alunite Ridge is located within the Toodoggone district in the Stikine terrane of northeastern BC (Figure 2). The Toodoggone district hosts a number of preserved Early Jurassic high- and low-sulphidation epithermal-type deposits (e.g., Alunite Ridge, Brenda, Shasta, Lawyers) with advanced argillic-alteration zones (Diakow et al., 1993; Bouzari et al., 2019). These deposits are hosted by a thick (>2 km) succession of Early Jurassic subaerial andesitic and dacitic volcanic rocks of the Toodoggone Formation (lower part of the Hazelton Group; Diakow et al., 1993). These and underlying strata were probably covered by thick successions (>4 km) of Jurassic and Cretaceous Bowser and Sustut basin clastic strata that protected and facili-

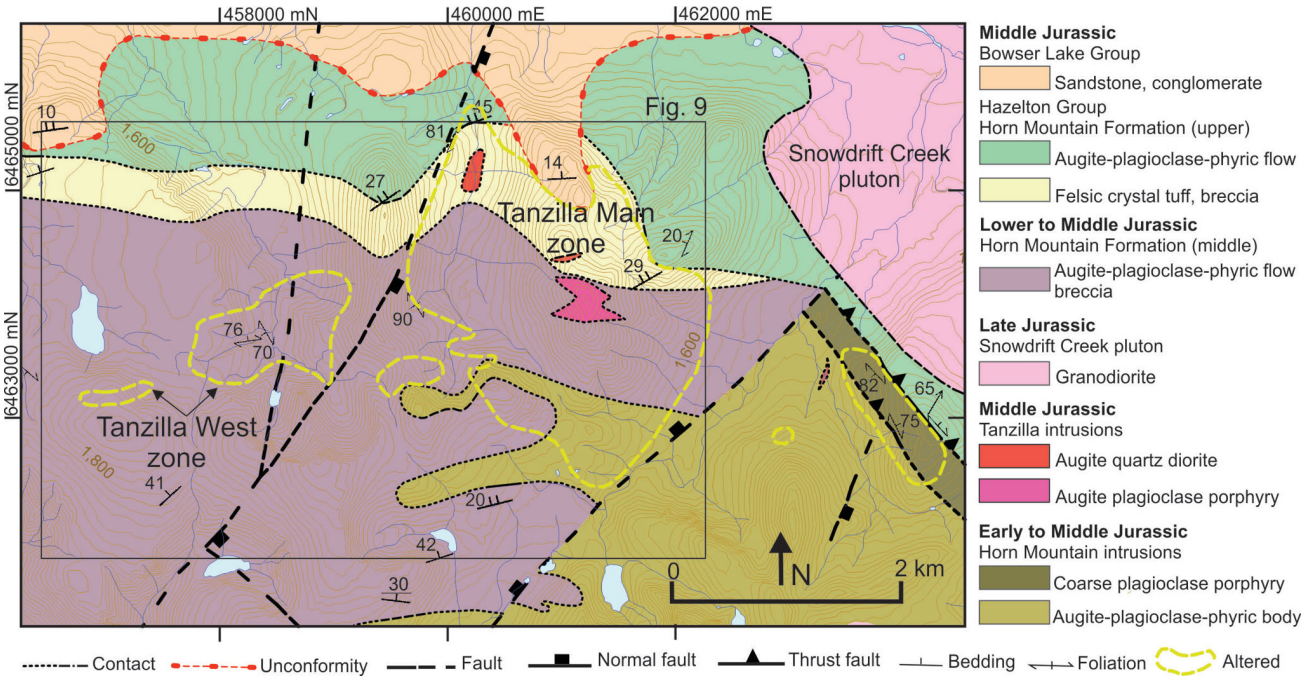

Figure 3. Geology of the Tanzilla study area (after van Straaten et al., 2017).

tated the preservation of the epithermal deposits during subsequent, post-Late Cretaceous uplift.

The Alunite Ridge area near Quartz Lake hosts several mineral occurrences, including Quartz Lake, Alunite Ridge, North Ridge and Sickle Creek. The Alunite Ridge and North Ridge occurrences form two northeast-trending ridges and the Quartz Lake occurrences are in the intervening valley. The underlying geology consists of lower Toodoggone Formation andesitic lava flows, tuffs, breccia and epiclastic rocks that are intruded by small dikes and stocks of monzonite (Figure 4). The Jock Creek monzonitic pluton forms a large body to the south and east.

Zones of intense alteration are northwest-trending and about 200 m wide. Gold mineralization occurs in a 10–15 m wide zone (Duuring et al., 2009) of silicified rock with quartz-alunite alteration, locally with vuggy textures and zones of buff-grey intense diaspore alteration (Bouzari et al., 2019). These are surrounded by quartz-sericite alteration, which locally contains pyrophyllite in zones that transition to the quartz-alunite alteration. Banded quartz veins with calcite and K-feldspar host low-sulphidation–type chalcopyrite-sphalerite-galena-pyrite mineralization and typically occur 100–300 m from the advanced argillic-altered zone at Alunite Ridge. Similar types of veins and mineralization, locally with amethystine quartz, occur at the base of the valley near Quartz Lake. Postmineralization monzonite dikes cut the alteration. A small granodiorite body at the Sofia prospect in the Toodoggone River valley is about 3 km northeast of Alunite Ridge, at an elevation of 1050 m asl (i.e., 700 m lower than Alunite Ridge). The granodiorite at Sofia hosts quartz-magnetite veins with K-feldspar alteration and traces of chalcopyrite, which are typical of deeper level porphyry mineralization (Bouzari et al., 2019).

Kemess North

The Kemess North porphyry mineralization is located about 6.5 km north of the main Kemess deposit (Kemess South) in the southern part of the Toodoggone district (Figure 2). Hostrocks at Kemess North include Upper Triassic Takla Group andesite/basaltic volcanic rocks locally overlain by Lower Jurassic Toodoggone Formation dacitic fragmental volcanic rocks (Figure 5). Toodoggone Formation volcaniclastic rocks crop out as prominent north-trending ridges or as isolated, fault-bounded blocks within Takla Group basalt. Several Early Jurassic stocks or dikes of quartz monzonite to quartz rhyolite composition of the Black Lake intrusive suite have intruded the volcanic succession. The area is dominated by horst-and-graben–style

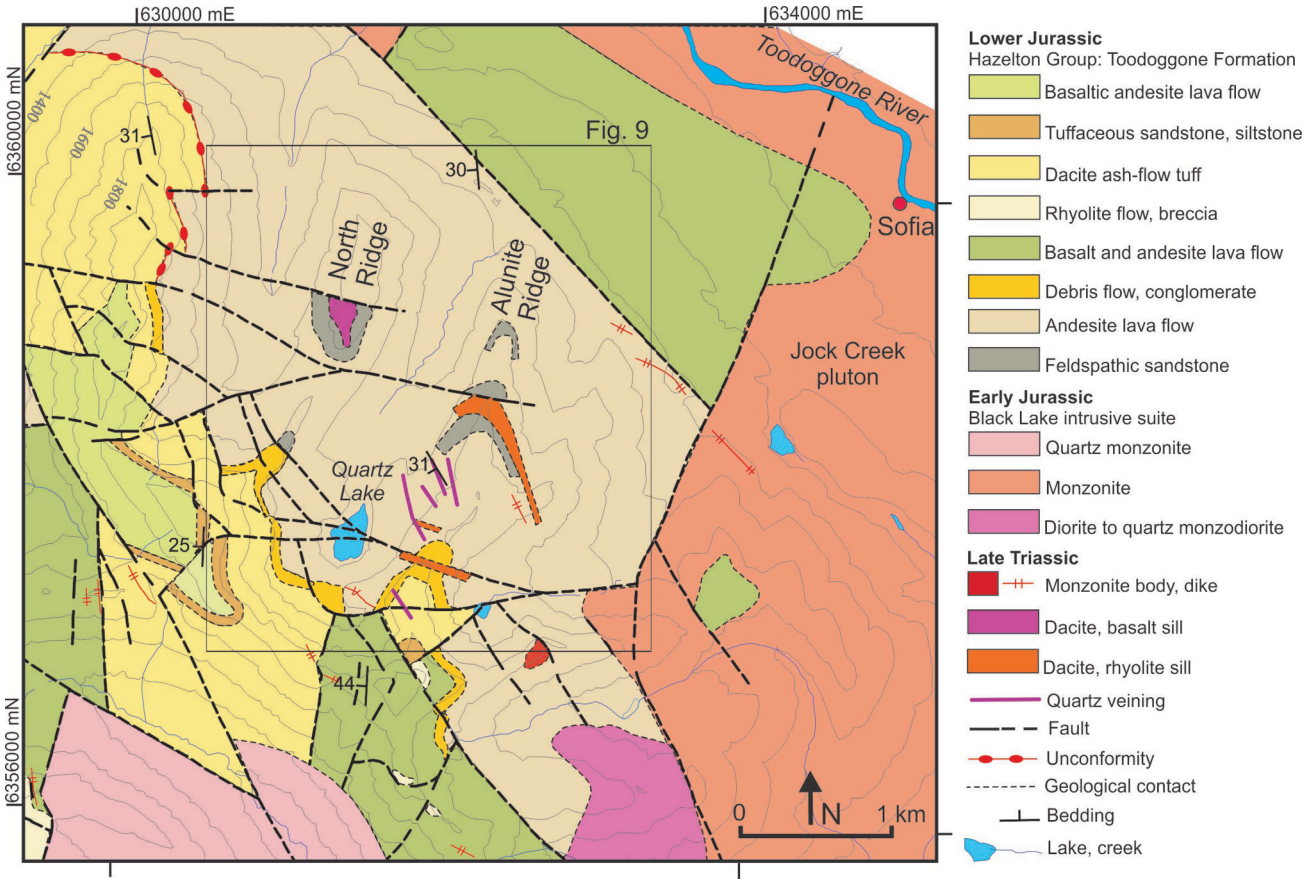

Figure 4. Geology of the Alunite Ridge study area (after Diakow et al., 2006).

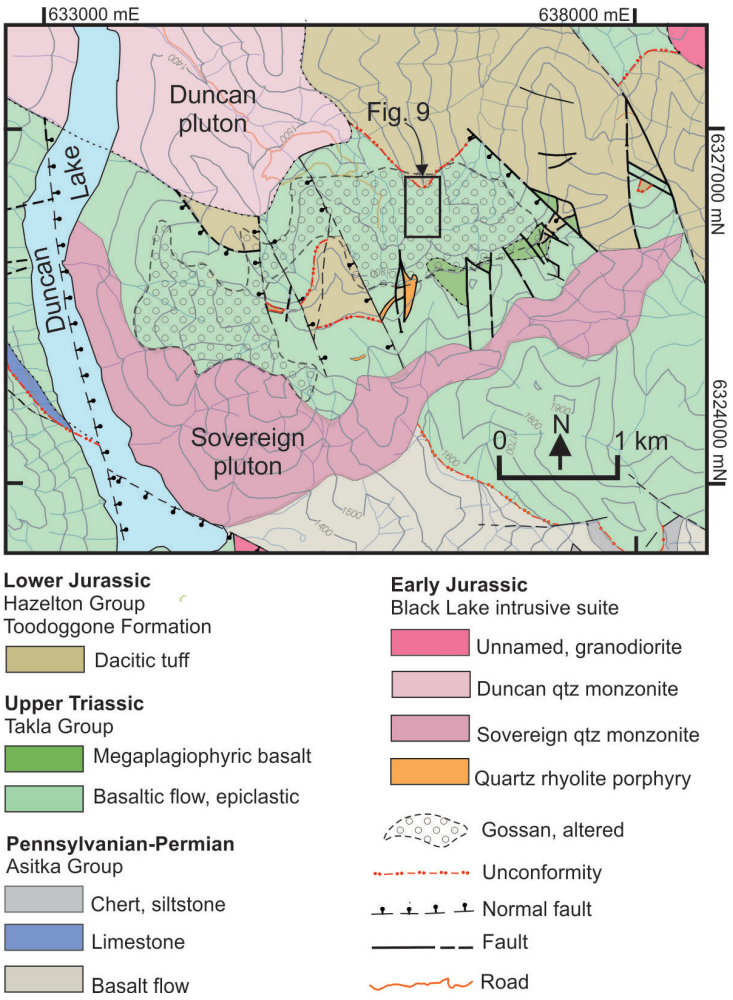

Figure 5. Geology of the Kemess North study area (after Diakow., 2001).

normal faulting, south-dipping thrust faulting and southwest-dipping dip-slip faulting (SRK Consulting Inc., 2016).

Porphyry-type veins and sulphide mineralization are centred around a quartz diorite body (ca. 202 Ma). The east-trending, south-dipping mineralization seems to have formed along faults. Associated phyllic-type alteration is characterized by very fine-grained quartz sericite-chlorite-pyrite alteration. The upper 80 m of the alteration is characterized by a zone of sulphate (anhydrite) leach and distinct depletion in calcium content of the rock (SRK Consulting Inc., 2016). At depth, the K-silicate alteration is characterized by quartz-magnetite stringers with decrease in the pyrite to chalcopyrite ratio. Early-stage veins include magnetite stringer veins and later quartz-magnetite-pyrite+chalcopyrite+molybdenite veins within the K-silicate alteration zone. The Main-stage quartz-pyrite+chalcopyrite± molybdenite veins occur with phyllic (sericite-quartz) alteration and yielded a Re-Os molybdenite age of 201.8 ±1.2 Ma (McKinley, 2006). These veins are cut by late-stage pyrite-chalcopyrite and anhydrite±pyrite±chalcopyrite veins, and postmineralization anhydrite and carbonate-zeolite veins (McKinley, 2006).

Fieldwork, Sampling and Analytical Work

Fieldwork was carried out during June and July 2019 at Tanzilla, Alunite Ridge and Kemess North. Access to the Tanzilla area was by helicopter from Dease Lake, and to Alunite Ridge by helicopter from a seasonable base at the Kemess mine. Access to the Kemess North area was by road from Kemess mine.

At Tanzilla, advanced alteration was mapped and sampled across a 3.5 km north–south profile and a 4 km east–west profile. A total of 54 samples were collected from surface outcrops. Drillhole TZ15-01 (Barresi and Luckman, 2016), which tested mineralization below the Main Ridge to the depth of 840 m (–60°) was examined, and 20 core samples were collected to characterize mineralization at depth. At Alunite Ridge, the footprint of alteration was mapped and sampled along three northeast-trending profiles with a total length of approximately 5 km in an area of 2 by 2 km. In to-

tal, 63 samples from surface outcrops ranging in elevation from 1908 to 1560 m asl and ten samples from drillhole SG-04-18 (SRK Consulting Inc., 2016) to a depth of 227 m below surface (1642 m asl) were collected. At Kemess North, advanced argillic alteration zone was mapped and sampled along a north-south profile of approximately 0.5 km. In total, 18 samples were collected from surface outcrops. Drillholes KN-01-12 and KN-02-09 (SRK Consulting Inc., 2016), which tested mineralization below the advanced argillic alteration to a depth of ~500 m below surface, were examined, and 44 core samples were collected to characterize alteration and mineralization at depth. In addition, from six other holes drilled into the advanced argillic-alteration zone, six samples were collected at a depth of approximately 150 m below surface to further compare with the samples from the surface outcrops.

To further characterize alteration assemblages, all samples were analyzed at MDRU using the tabletop version of the Terraspec® by Analytical Spectral Devices (ASD) Inc., with full-range visible and near-infrared (VNIR) and shortwave-infrared (SWIR) wavelengths for the range of 350–2500 nm. A sheet of Mylar™ was used as a standard, and this sheet was scanned at the start and end of every sampling day. Calibration with the white reflectance disk was completed at the start of every sampling day and re-calibrated every hour. The spectrum input was left at 100, and the white reference was set at 200. Spectra were visually inspected during collection, and where spectra were weak or absent, additional locations on the sample were scanned. Samples were processed with The Spectral Geologist (Commonwealth Scientific and Industrial Research Organisation, 2019) software for measuring spectral features such as wavelength position and crystallinity. Mineral identification and spectra quality assessment (e.g., noise and molecular water contamination) were performed using the SpecWin (Instrument Systems, 2019) software using the SpecMIN™ (Spectral Evolution, 2019) reference library.

All samples were cut into rock slabs and photographed for more detailed description. All samples are being processed for whole-rock geochemical analysis and selected samples for thin-section preparation. The results of these analyses will be provided in a subsequent publication.

Field Observations

Tanzilla

At Tanzilla, advanced argillic alteration covers an area of 5 by 2 km at the western margin of the Snowdrift Creek pluton (Figure 3; van Straaten and Nelson, 2016). The main Tanzilla hill alteration occurs in an area of 2 by 2 km (Figures 3, 6a, b), referred to here as the 'Main zone', but similar types of alteration zones occur 2–3 km to the west, referred to here as the 'West zone'. The hostrocks to the Tanzilla alteration are augite-plagioclase-phyric volcanic rocks with altered mafic minerals (Figure 6c), locally tuff and volcanic breccia (Figure 6d) of the Horn Mountain Formation. Coarse hornblende-plagioclase porphyry (Figure 6e) and feldspar porphyry dikes, with fresh texture or weak alteration, cut the strongly altered volcanic rocks. These porphyry dikes are interpreted as part of Snowdrift Creek pluton (van Straaten and Gibson, 2017).

The Tanzilla area is characterized by a large (>2 km) pale green quartz-green sericite-chlorite-pyrite alteration zone (Figure 6f) that grades to a quartz-white sericite-pyrite assemblage (Figure 6g) toward the zones of advanced argillic alteration. Coarse sericite or muscovite occurs locally within this assemblage. In the Main zone, copper oxides occur with narrow jarosite-goethite veinlets. In more central locations and commonly at higher elevations, the alteration is characterized by highly silicified rock (Figure 6h), with remnants of sericite, pyrite and locally with abundant clays typical of advanced argillic alteration. The latter alteration is developed along structures and locally contains narrow zones of high sulphidation-type pyrite-grey sulphide mineralization. Bladed calcite, coated by quartz and sulphides, now mostly leached, occurs within the silicified rocks of the Main zone (Figure 6k), which suggests a boiling environment at shallow levels.

Alteration outside of the quartz-green sericite-chlorite-pyrite is dominantly darker green chlorite-sericite-pyrite (Figure 6d, i) and more distal patchy chlorite-epidote alteration occurs within the volcanic rocks (Figure 6j).

Porphyry-type alteration occurs in a diorite body at approximately 780 m in drillhole TZ15-01 (Barresi and Luckman, 2016), with K-silicate alteration and weak sulphide mineralization cutting the chlorite-sericite–altered volcanic rock. A similar type of alteration occurs in a coarse-grained pinkish monzodiorite(?) body, approximately 50 m wide, cut by quartz-magnetite-(trace sulphide) veins, about 1.8 km south of the Main zone (Figure 6b, l). Remnants of pervasive, fine-grained biotite alteration at depth in the drillhole, largely replaced by chlorite and sericite, point to an earlier, larger porphyry-related potassic alteration. Thus, the K-silicate–altered monzodiorite and diorite may represent shallower and probably younger manifestations of such an intrusive body at depth in the area, which generated the advanced argillic alteration at the shallowest level.

Alunite Ridge

Advanced argillic alteration at Alunite Ridge occurs for over 2 km along a northeast-trending ridge. Similar types of alteration occur in the North Ridge occurrence approximately 1 km to the northwest (Figure 4). Field observations indicate that the central part of the Alunite Ridge (Figure 7a) is characterized by an alteration zone of strong sili-

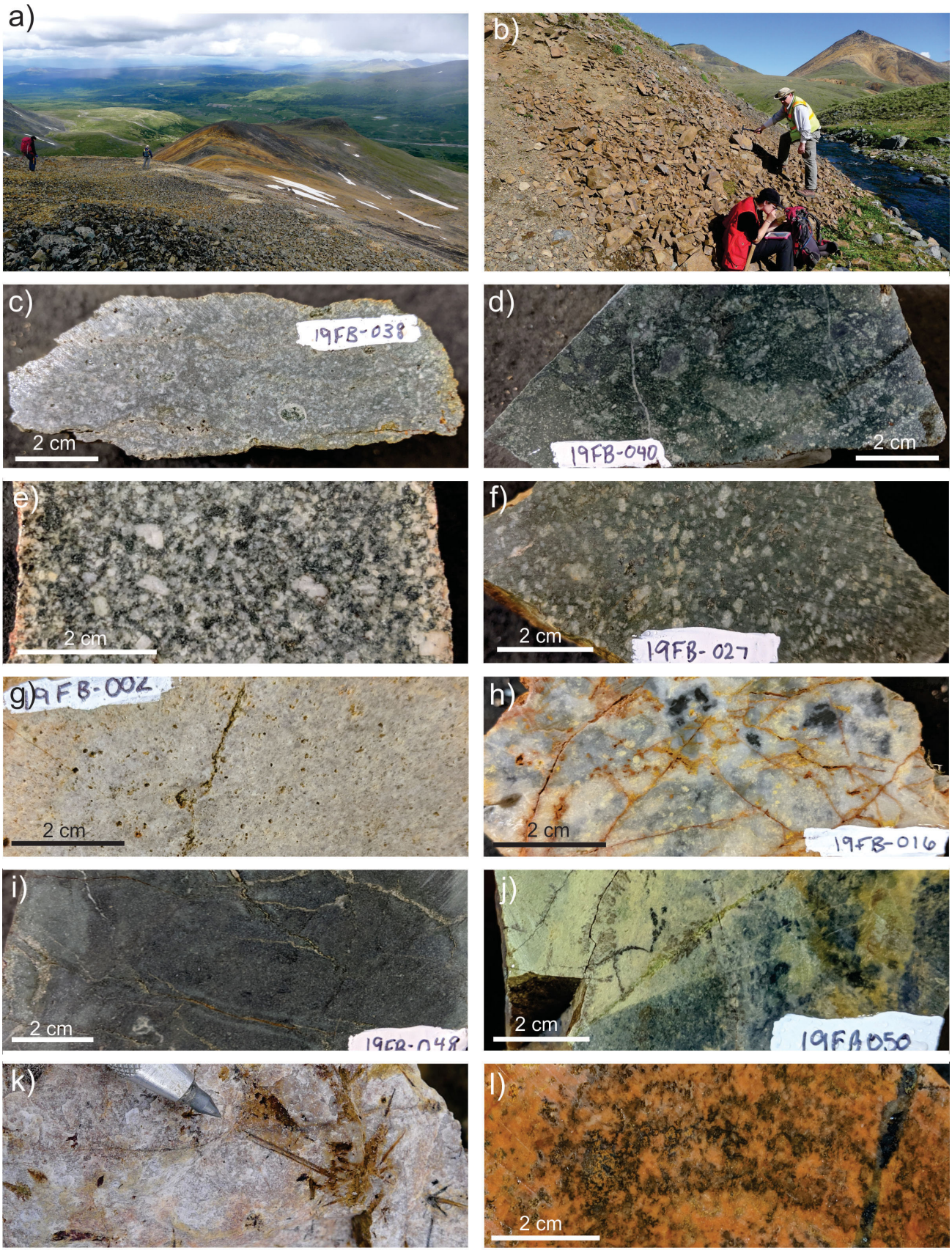
a)
b)
c)
19FB-038
2 cm
d)
19FB-040
2 cm
e)
2 cm
f)
2 cm
19FB-027
g)
2 cm
h)
2 cm
19FB-016
i)
2 cm
j)
2 cm
k)
l)
2 cm

Figure 6. Hostrock and alteration samples from the Tanzilla study area: **a)** looking north to the Tanzilla northern ridge characterized by limonite-stained volcanic outcrops and, in the foreground, an outcrop of weakly altered hornblende-plagioclase porphyry dike; **b)** looking north to the Tanzilla Main zone (in the background), the outcrop in the foreground is a small body of monzodiorite with pervasive biotite and K-feldspar alteration cut by quartz-magnetite-(chalcopyrite) veinlets; **c)** sample of the main hostrock at Tanzilla, which is a plagioclase-phyric volcanic rock with altered mafic minerals; **d)** volcanic breccia with chlorite alteration; **e)** coarse-grained hornblende-plagioclase porphyry with weak chlorite alteration; **f)** sample of pale green quartz-green sericite-chlorite-pyrite altered rock; **g)** sample of quartz-white sericite-pyrite altered rock; **h)** sample showing strong silicification and silica flooding with remnants of sericite alteration; **i)** sample of dark green chlorite-sericite-pyrite alteration; **j)** sample of chlorite-epidote alteration; **k)** silicified bladed calcite, coated by sulphides, now mostly leached; **l)** pinkish monzodiorite(?) cut by quartz-magnetite-(trace sulphide) veins.

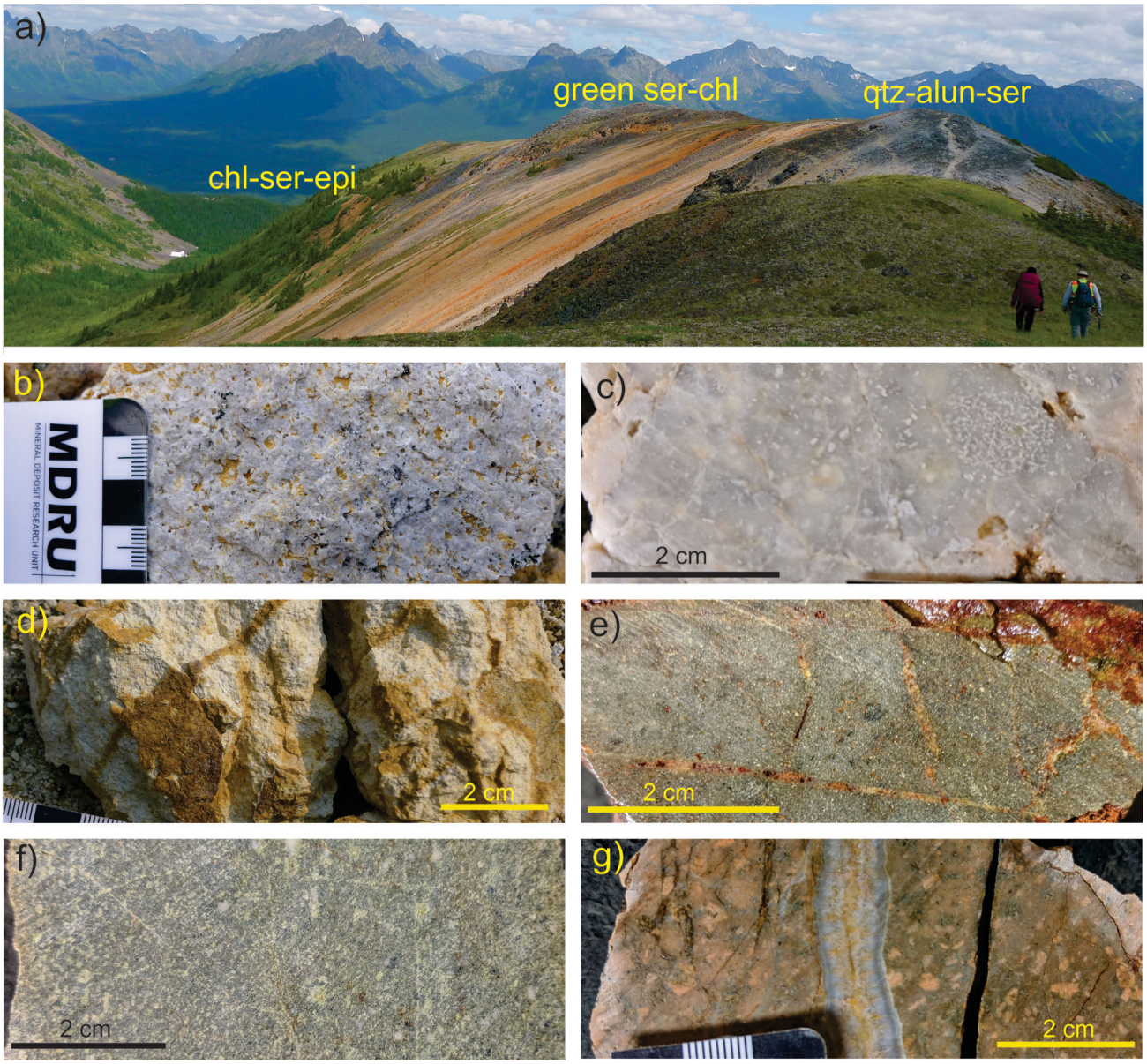

Figure 7. Hostrock and alteration samples from the Alunite Ridge study area: **a)** looking northeast to the Alunite Ridge, showing a grey silicified rock-alunite-sericite (qtz-alun-ser)–rich zone followed by limonite-stained green sericite-chlorite (green ser-chl) alteration and chlorite-sericite-epidote (chl-ser-epi) alteration occurring more distally; **b)** sample of strongly silicified rock displaying vuggy texture; **c)** host volcanic rock with remnants of plagioclase phenocrysts overprinted by silicification, alunite and white sericite alteration; **d)** clay alteration with stockwork of oxidized sulphide veinlets; **e)** pale green sericite-chlorite alteration with disseminated and thin veinlets of pyrite largely oxidized to jarosite; **f)** chlorite-sericite-epidote alteration; **g)** banded quartz and carbonate vein cuts pervasive pink K-feldspar–altered plagioclase porphyry.

cification, locally displaying vuggy texture (Figure 7b). Alunite and white sericite (Figure 7c) occur locally in this zone with clay (Figure 7d). This zone is surrounded by an alteration zone of pale green sericite- chlorite with disseminated and thin veinlets of pyrite largely oxidized to jarosite (Figure 7e). Locally, coarser grained sericite occurs and veins are typically thin quartz veinlets, locally with barite. This alteration gradually transitions to the north and east at lower elevations (e.g., below 1700 m asl) to darker green alteration of chlorite-sericite and locally epidote occurs more distally (Figure 7f). Green sericite-chlorite and chlorite-sericite alteration zones in the southern parts of the Alunite Ridge are cut by breccia as well as banded quartz and carbonate veins, locally with pervasive pink K-feldspar (Figure 7g) characterizing a low-sulphidation-type alteration overprint.

Kemess North

Advanced argillic to phyllic alteration at Kemess North is largely hosted by basaltic plagioclase-phyric volcanic rocks of the Takla Group, which are in fault contact with dacitic tuff of the Toodoggone Formation of the Hazelton Group. The strongly altered rocks form a large orange gossan over an area of 3 by 1 km (Figure 5). During the fieldwork, samples were recovered from along an approximately 0.5 m section of a north-trending ridge above the hypogene mineralization (Figure 8a). The alteration zone exposed on the surface is distinctly zoned from south to north. In the southern parts of the ridge, alteration is charac-

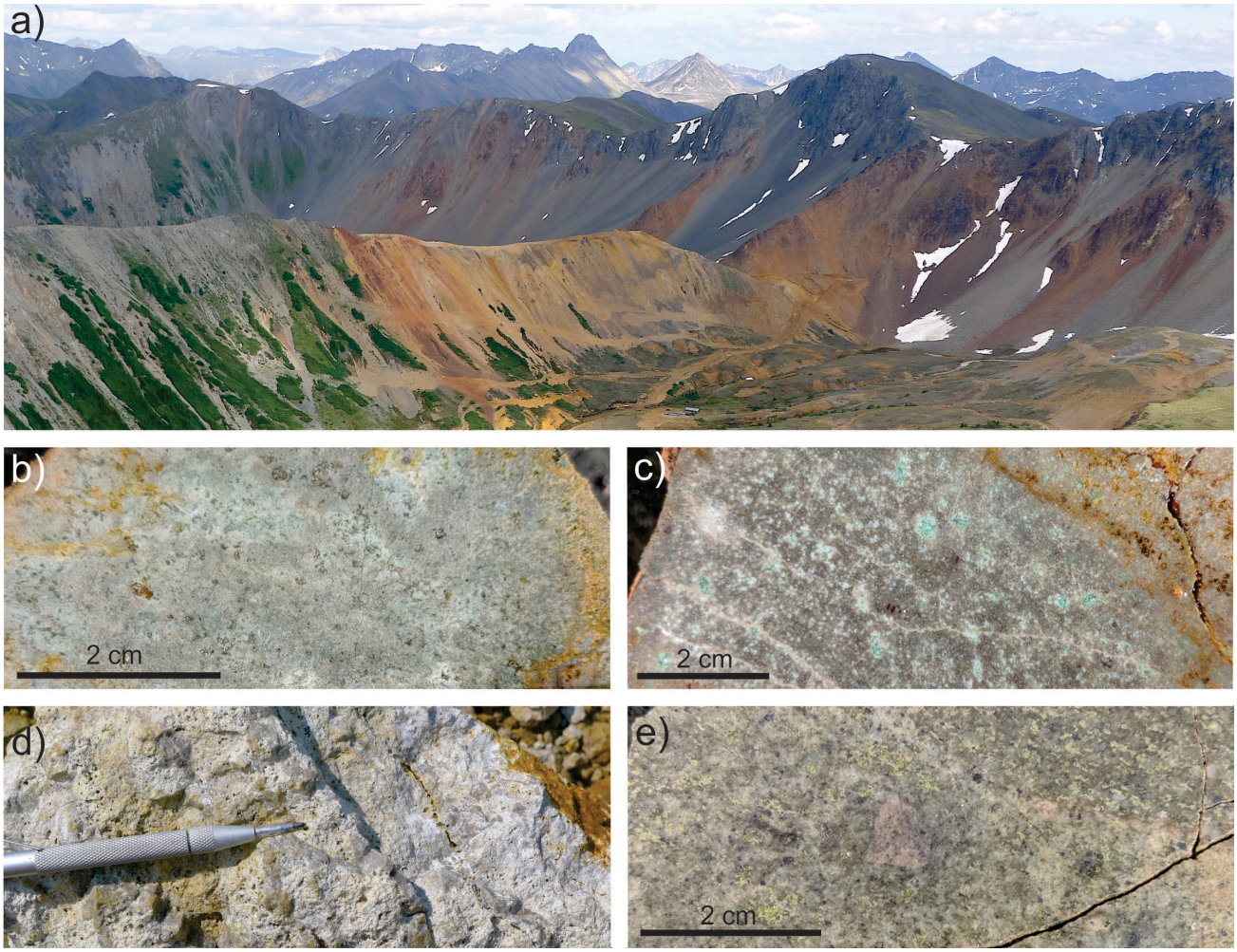

Figure 8. Hostrock and alteration samples from the Kemess North study area: **a)** looking southeast to the Kemess North ridge, showing strongly altered Takla Group volcanic rocks with orange gossan colouration; **b)** pale green altered rock characterized by a green sericite-chlorite-pyrite assemblage; **c)** green-grey sericite-pyrite assemblage; **d)** grey-white sericite-clay-pyrite with strong pervasive silicification and quartz veining; **e)** chlorite-epidote altered volcanic rock of the Toodoggone Formation.

terized by green sericite-chlorite-pyrite, which appears as a pale greenish rock (Figure 8b). This gradually transitions northward to a green-grey sericite-pyrite assemblage (Figure 8c) and then to a grey-white sericite-clay-pyrite typically with pervasive silicification and quartz veins (Figure 8d). The latter is in fault contact with the chlorite-epidote–altered volcanic rocks of the Toodoggone Formation to the north (Figure 8e). Pyrite is abundant (>2%) occurring as dissemination and stockwork veining with quartz. Sulphides are oxidized along fractures producing the rusty outcrops. Locally, minor copper oxides occur, which suggests that hypogene chalcopyrite is leached, but abundant pyrite remains preserved and is only coated by jarosite.

Similar alteration zones occur at depth as indicated in the drillholes. The alteration zone beneath the advanced argillic-alteration zone is quartz-green sericite-(magnetite-hematite) with disseminated pyrite and chalcopyrite. The chlorite content increases with depth and the alteration assemblage becomes darker green. Granular quartz veins with chalcopyrite, pyrite and magnetite (cp > py) occur within the green sericite-chlorite alteration zone. Zones of white sericite with abundant pyrite locally cut and overprint the green sericite-chlorite alteration, indicating that white sericite-pyrite alteration is well developed at shallow levels and overprints the sericite-chlorite alteration at depth. The K-silicate alteration is characterized by pink K-feldspar, typically along fractures with quartz, and variable amounts of pyrite and chalcopyrite occur below the sericite-chlorite zone. Epidote is locally present with K-feldspar, which indicates that the K-silicate alteration transitions toward propylitic-type alteration. It is apparent that both K-silicate and sericite-chlorite alteration zones host copper and gold mineralization at Kemess North.

SWIR Results

Alteration assemblages were further characterized by evaluating SWIR mineralogy. Results of samples collected from surface outcrops are shown in Figure 9, and those for samples collected from drillholes will be discussed in a future publication.

White micas (muscovite or illite) are a typical alteration phase at all the studied sites (Figure 9a). At Tanzilla, muscovite is dominant in the Main zone and locally in bodies of altered rocks in the West zone. White mica alteration at Alunite Ridge and Kemess North is characterized dominantly by illite. Muscovite occurs only in the southern part of the North Ridge. Pyrophyllite occurs in the Main zone at Tanzilla and within the quartz-alunite alteration zone at Alunite Ridge (Figure 9a).

The composition of the white mica (Figure 9b) is described as paragonitic (Na-rich), muscovite/illite (K-rich) and phengitic (Mg-Fe-rich). At Tanzilla, both K-rich muscovite/illite and paragonite are abundant, whereas phengitic micas occur locally. At Alunite Ridge, K-rich illite is abundant, especially with the quartz-alunite-white sericite–altered rock, whereas phengitic illite is more abundant with the pale green sericite-chlorite alteration. At Kemess North, paragonitic illite occurs in the south, whereas K-rich illite occurs to the north, thus correlating more closely with the white-sericite alteration. The occurrence of K-rich white mica is attributed to fluids with lower pH relative to the fluids responsible for the formation of the phengitic micas.

The sericite crystallinity index, calculated from the ratio of 2200 and 1900 nm wavelength depths, shows that white micas at the Tanzilla Main zone are strongly crystalline (>2.0), whereas farther south and at the West zone they are less crystalline (<1.5; Figure 9c). At Alunite Ridge, the crystallinity varies from moderate (ca. 1–1.5) to poor (<1). The latter seems to be more common distally within the sericite-chlorite and chlorite-epidote alteration zones. At Kemess North, white mica crystallinity increases from south (ca. 1) to north (>2). The more highly crystalline sericite occurs with the white-grey sericite alteration (Figure 9c).

Chlorite was identified in most rock samples and displays a wide range of compositions, from Mg rich to Fe-Mg rich (Figure 9d). No obvious trends in chlorite composition with alteration type is recognized. However, locally there is a correlation between the occurrence of phengitic mica and that of Fe-Mg chlorite. More petrography work is planned to study chlorite occurrence, and its relationship to alteration and hostrock types.

Clay minerals are not typical at Tanzilla, whereas dickite and kaolinite occur at Alunite Ridge with the alunite-white sericite zone and, at Kemess North, with the grey-white sericite alteration zone (Figure 9e). The SWIR analyses also identified topaz occurring locally with pyrophyllite or alunite at the Tanzilla Main zone (Figure 9f).

Conclusions and Further Work

Field and SWIR data show that advanced argillic alteration in the studied sites is distinctly zoned. The central parts of the advanced argillic-alteration zone are typically characterized by strong silicification, both as quartz flooding and veining. Alunite, pyrophyllite and topaz locally occur with the silicified rock. Vuggy textures occur, but are not widespread. Sericite and clay minerals also occur. Collectively, they form an alteration assemblage of quartz-white to grey sericite-(clay). Clay minerals include both kaolinite and dickite, and there is a reverse correlation between abundance of clay minerals and abundance of coarse, especially strongly crystalline sericite. This is interpreted as a fluid-temperature control characterizing vertical zonation of the alteration profile. Clay-rich alteration assemblages, espe-

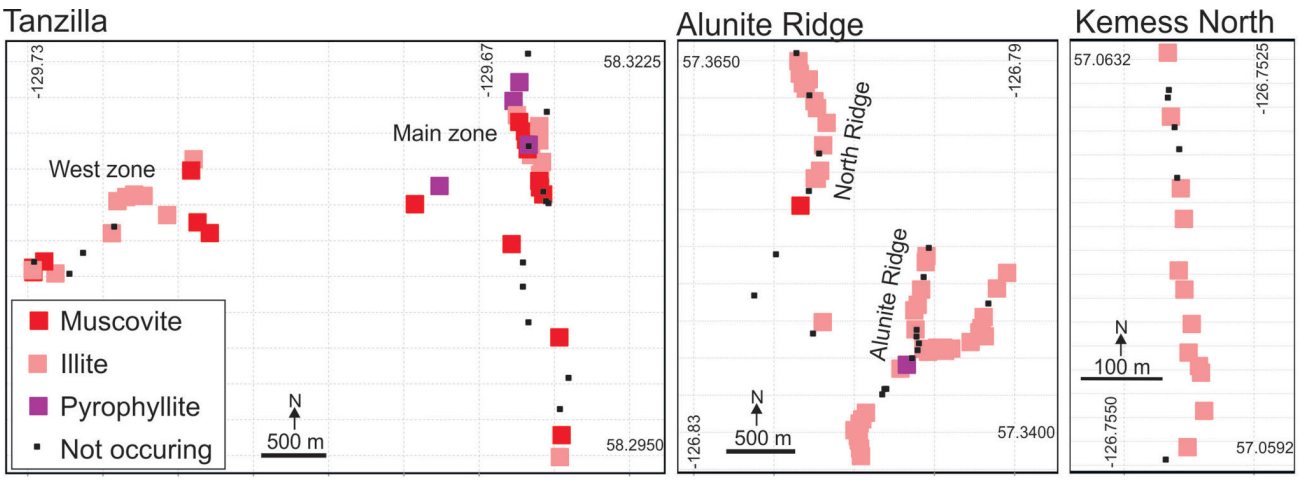

a) White mica and pyrophyllite

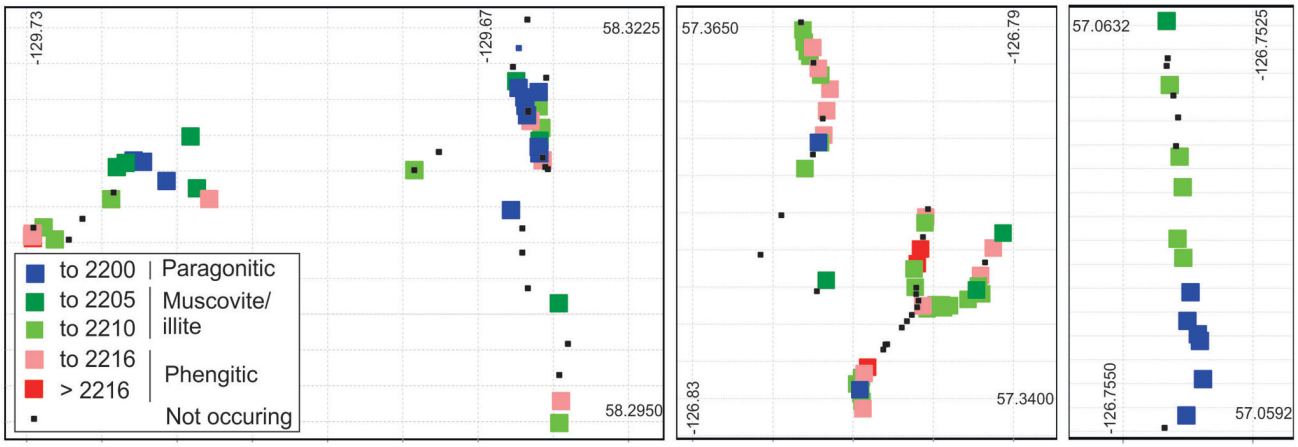

b) White mica, 2200 nm wavelength

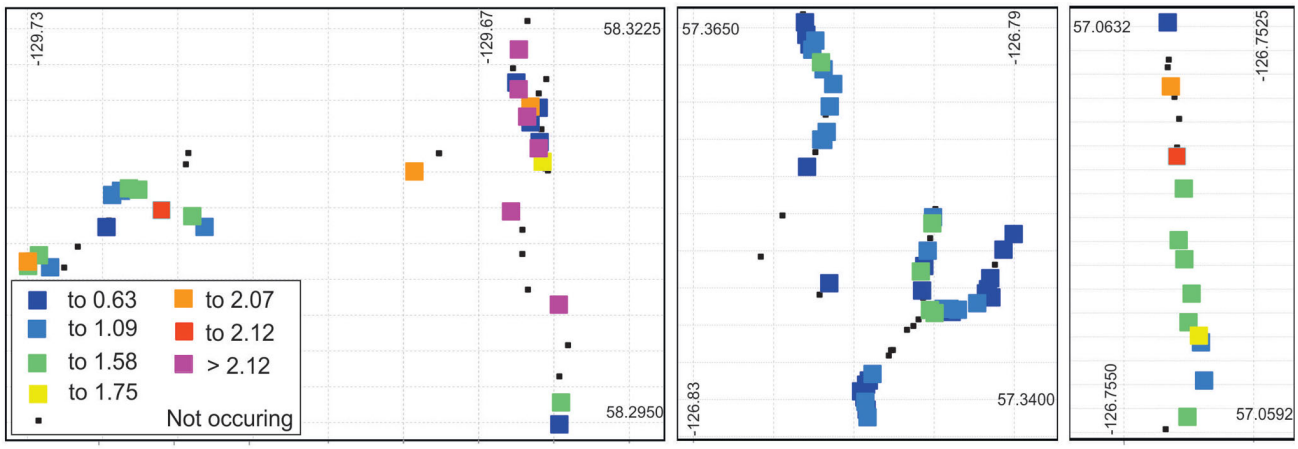

c) White mica, crystallinity index

Figure 9 [this page and the next]. Diagrams showing mineral phases and compositions identified by shortwave-infrared analyses at the Tanzilla, Alunite Ridge and Kemess North study areas: **a)** distribution of white mica and pyrophyllite; **b)** composition of white micas; **c)** crystallinity of white micas; **d)** distribution and composition of chlorite; **e)** distribution of clay minerals; **f)** distribution of alunite and topaz. Small black squares represent mineral of interest not occurring in the sample location.

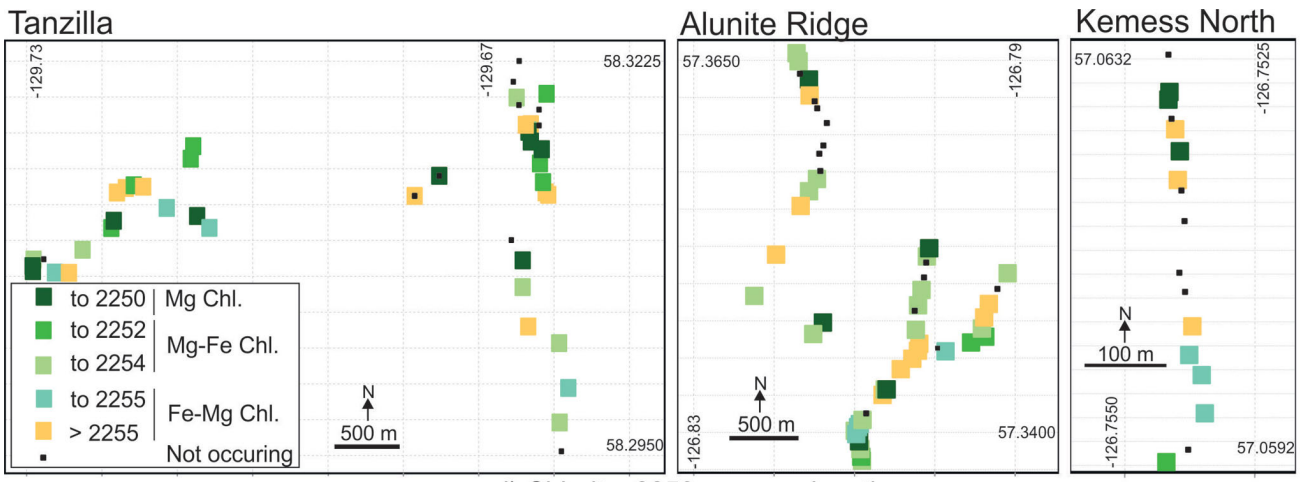

d) Chlorite, 2250 nm wavelength

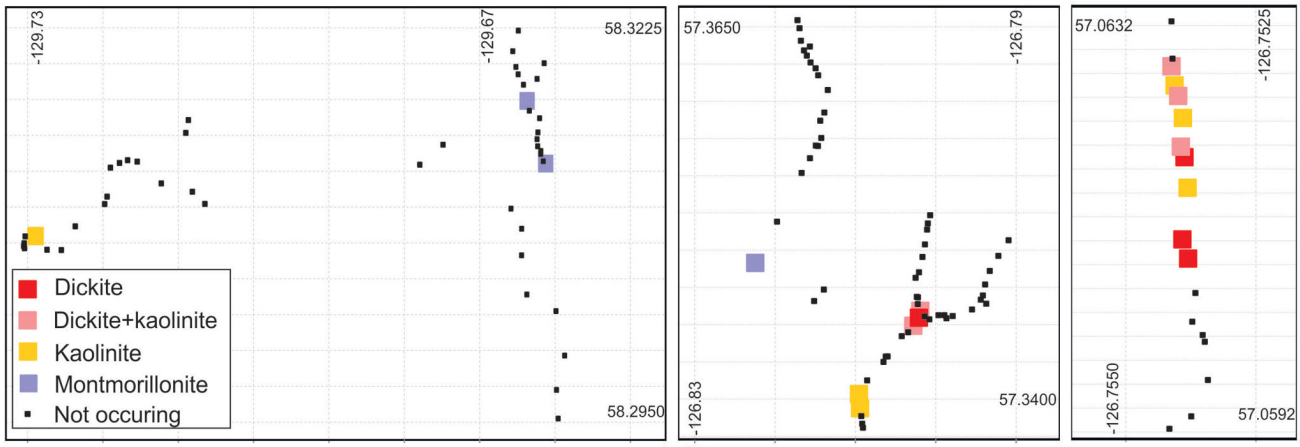

e) Clays

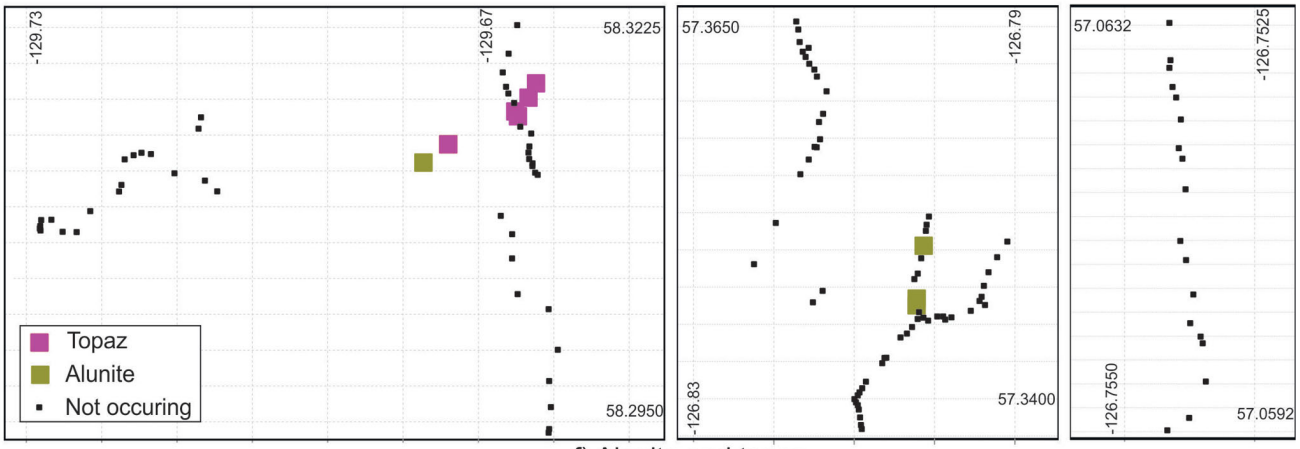

f) Alunite and topaz

cially kaolinite, are less abundant than those consisting of sericite and chlorite. This is interpreted as a hostrock-effect control by the dominantly mafic character of the volcanic rocks of the Takla or Hazelton groups, which buffered the fluids.

Alteration outside of the quartz-white to grey sericite-(clay) zone is characterized by a pale greenish rock containing assemblages of quartz-green sericite-chlorite. The sericite is typically K-rich and reflects the acidic environment of formation. The size of this alteration varies laterally from a few hundred metres to over two kilometres. The crystallinity of the sericite increases toward and within the quartz-white to grey sericite-(clay) zone, but the chlorite compositions do not show distinct-scale variations. More distally, the proportion of the chlorite increases to form green chlorite-sericite alteration and chlorite-epidote-(sericite) more distally.

These field observations and the SWIR mineral identifications provide a framework to further characterize the mineralogical and chemical compositions of zoned, advanced argillic-alteration systems. Samples collected from drillholes will further characterize vertical zonation. Detailed petrography, X-ray diffraction and scanning electron microscope work is planned for mineral characterization. Chemical analyses and measuring physical rock properties (e.g., rock density and magnetic susceptibility) will further characterize each alteration zone. Cathodoluminescence studies are planned to characterize quartz from various alteration stages or zones. Together, these data will be used to establish a field and laboratory toolkit for exploration.

Acknowledgments

Geoscience BC is thanked for its financial contribution in support of this project. Kaizen Discovery Inc. gave permission to visit the Tanzilla property and sample drillcore. Centerra Gold provided access to Kemess North and drillcore, as well as accommodation at the Kemess mine. The authors thank R. Billingsley for giving them permission to visit the Alunite Ridge property. Field assistance was provided by Z. Boileau and F. Bhanji helped draft the maps. They also thank H. Leal-Mejía of the Mineral Deposit Research Unit of The University of British Columbia for his review and comments on this paper.

References

Barresi, T. and Luckman, N. (2016): Diamond drilling report on the Tanzilla property, northwestern British Columbia; BC Ministry of Energy, Mines and Petroleum Resources, Assessment Report 36431, 45 p., URL <https://aris.empr.gov.bc.ca/ArisReports/36431.PDF> [December 2019].

Barresi, T., Bradford, J. and Luckman, N. (2014): 2014 Diamond drilling report on the Tanzilla property, northwestern British Columbia; BC Ministry of Energy, Mines and Petroleum Resources, Assessment Report 35471, 46 p., URL <https://aris.empr.gov.bc.ca/ARISReports/35471.PDF> [May 2019].

Bissig, T. and Cooke, D.R. (2014): Introduction to the special issue devoted to alkalic porphyry Cu-Au and epithermal Au deposits; Economic Geology, v. 109, p. 819–825.

Bouzari, F., Bissig, T., Hart, C.J.R. and Leal-Mejía, H. (2019): An exploration framework for porphyry to epithermal transitions in the Toodoggone mineral district (94E); Geoscience BC Report 2019-08, MDRU Publication 424, 101 p., URL <http://www.geosciencebc.com/wp-content/uploads/2019/11/Geoscience-BC-Report-2019-08.pdf> [October 2019].

Bouzari, F., Hart, J.R.C., Bissig, T. and Shaun, B. (2016): Hydrothermal alteration revealed by apatite luminescence and chemistry: a potential indicator mineral for exploring covered porphyry copper deposits; Economic Geology, v. 111. p. 1397–1410.

Chang, Z., Hedenquist, J.W., White, N.C., Cooke, D.R., Roach, M., Deyell, C.L. and Cuison, A.L. (2011): Exploration tools for linked porphyry and epithermal deposits: example from the Mankayan intrusion-centered Cu-Au district, Luzon, Philippines; Economic Geology, v. 106, p. 1365–1398.

Commonwealth Scientific and Industrial Research Organisation (2019): The Spectral Geologist (TSG™): the industry standard tool for the mineralogical analysis VIS/NIR/SWIR/MIR and TIR reflectance spectra, release 8.0.5.1, Commonwealth Scientific and Industrial Research Organisation, software application, URL <https://research.csiro.au/thespectralgeologist/> [November 2019].

Deyell, C.L. and Dipple, G.M. (2005): Equilibrium mineral–fluid calculations and their application to the solid solution between alunite and natroalunite in the El Indio–Pascua belt of Chile and Argentina; Chemical Geology, v. 215, p. 219–234.

Deyell, C.L., Thompson, J.F.H., Friedman, R.M. and Groat, L.A. (2000): Age and origin of advanced argillic alteration zones and related exotic limonite deposits in the Limonite Creek area, central British Columbia; Canadian Journal of Earth Sciences, v. 37, p. 1093–1107.

Diakow, L.J. (2001): Geology of the southern Toodoggone River and northern McConnell Creek map areas, north-central British Columbia (parts of NTS 94E/2, 94D/15 and 94D16); BC Ministry of Energy, Mines and Petroleum Resources, BC Geological Survey, Geoscience Map 2001-1, scale 1:50 000, URL <http://cmscontent.nrs.gov.bc.ca/geoscience/PublicationCatalogue/GeoscienceMap/BCGS_GM2001-01.pdf> [May 2019].

Diakow, L.J., Nixon, G.T., Rhodes. R. and van Bui, P. (2006): Geology of the central Toodoggone River map area, north-central British Columbia (parts of NTS 94E/2, 6, 7, 10 and 11); BC Ministry of Energy, Mines and Petroleum Resources, Open file map 2006-6, scale 1:50 000, URL <http://cmscontent.nrs.gov.bc.ca/geoscience/PublicationCatalogue/GeoscienceMap/BCGS_GM2006-06.pdf> [May 2019].

Diakow, L.J., Panteleyev, A. and Schroeter, T.G. (1993): Geology of the early Jurassic Toodoggone Formation and gold-silver deposits in the Toodoggone river map area, northern British Columbia; BC Ministry of Energy, Mines and Petroleum Resources, Bulletin 86, 72 p., URL <http://cmscontent.nrs.gov.bc.ca/geoscience/PublicationCatalogue/Bulletin/BCGS_B086.pdf> [May 2019].

Duuring, P., Rowins, S.M., McKinley, B.S.M., Dickinson, J.M., Diakow, L.J., Kim, Y.-S. and Creaser, R.A. (2009): Examining potential genetic links between Jurassic porphyry Cu-

Au±Mo and epithermal Au±Ag mineralization in the Toodoggone district of North-Central British Columbia, Canada; Mineralium Deposita, v. 44, p. 463–496.

Halley, S.W., Dilles, J.H. and Tosdal, R.M. (2015): Footprints: hydrothermal alteration and geochemical dispersion around porphyry copper deposits, Society of Economic Geologists, Newsletter, no. 100.

Hedenquist, J.W. and Taran, Y.A. (2013): Modeling the formation of advanced argillic lithocaps: volcanic vapor condensation above porphyry intrusions; Economic Geology, v. 108, p. 1523–1540.

Heinrich, C.A. (2007): Fluid-fluid interactions in magmatic-hydrothermal ore formation; Reviews in Mineralogy and Geochemistry, v. 65, p. 363–387.

Heinrich, C.A., Driesner, T., Stefánsson, A. and Seward, T.M. (2004): Magmatic vapor contraction and the transport of gold from the porphyry environment to epithermal ore deposits; Geology, v. 32, p. 761–764.

Instrument Systems (2019): SpecWin spectral software; Instrument Systems, software for spectrometer operation, URL <http://www.instrumentsystems.com/products/spectral-software/specwin-pro/> [November 2019].

Lesher, M., Hannington, M., Galley, A., Ansdell, K., Astic, T, Banerjee, N., Beauchamp, S., Beaudoin, G., Bertelli, M., Bérubé, C., Beyer, S., Blacklock, N., Byrne, K., Cheng, L.-Z., Chouinard, R., Chouteau, M., Clark, J., D'Angelo, M., Darijani, M., Devine, M. et al. (2017): Integrated multi-parameter exploration footprints of the Canadian Malartic disseminated Au, McArthur River–Millennium unconformity U, and Highland Valley porphyry Cu deposits: preliminary results from the NSERC-CMIC Mineral Exploration Footprints Research Institute; *in* Proceedings of Exploration 17: Sixth Decennial International Conference on Mineral Exploration, V. Tschirhart and M.D. Thomas (ed.), p. 325–347, URL <https://www.semanticscholar.org/paper/Integrated-Multi-Parameter-Exploration-Footprints-%2C-Lesher-D'Angelo/414a5bd2152876577f69dd53b7276a8441a612f0> [October 2019].

Luckman, N., Celiz, M.A.D., Wetherup, S. and Walcott, P. (2013): Induced polarization, terraspec and structural surveys on the Tanzilla property; BC Ministry of Energy, Mines and Petroleum Resources, Assessment Report 34 550, 24 p., URL <https://aris.empr.gov.bc.ca/ArisReports/34550.PDF> [May 2019].

McKinley, B.S.M. (2006): Geological characteristics and genesis of the Kemess North porphyry Au–Cu–Mo deposit, Toodoggone district, north-central British Columbia, Canada; M.Sc. thesis, University of British Columbia, 136 p., URL <https://open.library.ubc.ca/cIRcle/collections/ubctheses/24/items/1.0052897> [May 2019].

Nelson, J. and Mihalynuk, M. (1993): Cache Creek ocean: closure or enclosure?; Geology, v. 21, p. 173–176.

Panteleyev, A. (1992): Copper-gold-silver deposits transitional between subvolcanic porphyry and epithermal environments; *in* Geological Fieldwork 1991, BC Ministry of Energy, Mines and Petroleum Resources, BC Geological Survey, Paper 1992-1, p. 229–234, URL <https://www2.gov.bc.ca/gov/content/industry/mineral-exploration-mining/british-columbia-geological-survey/publications/fieldwork> [May 2019].

Panteleyev, A. and Koyanagi, V.M. (1994): Advanced argillic alteration in Bonanza volcanic rocks, northern Vancouver Island – lithologic and permeability controls; *in* Geological 1993, BC Ministry of Energy, Mines and Petroleum Resources, BC Geological Survey, Paper 1994-1, p. 101–110, URL <https://www2.gov.bc.ca/gov/content/industry/mineral-exploration-mining/british-columbia-geological-survey/publications/fieldwork> [May 2019].

Shearer, J.T. (2004): Kaolin and silica resources in advanced argillic (acid sulphate) alteration zones, northern Vancouver Island, British Columbia, Canada; in Industrial Minerals with Emphasis on Western North America, G.J. Simandl, N.J. McMillan and N. Robinson (ed.), BC Ministry of Energy, Mines and Petroleum Resources, Paper 2004-02, p. 31–32, URL <http://cmscontent.nrs.gov.bc.ca/geoscience/PublicationCatalogue/Paper/BCGS_P2004-02-06_Shearer.pdf> [May 2019].

Sillitoe, R.H. (1993). Epithermal models: genetic types, geometrical controls and shallow features; *in* Mineral Deposit Modelling, R.V. Kirkham, W.D. Sinclair, R.J. Thorpe and J.M. Duke (ed.), Geological Association of Canada, Special Paper 40, p. 403-417.

Sillitoe, R.H. (2000): Gold-rich porphyry deposits: descriptive and genetic models and their role in exploration and discovery; *in* Gold in 2000, S.G. Hagemann and P.E. Brown (ed.), Reviews in Economic Geology, v. 13, p. 315–345.

Sillitoe, R.H. (2010): Porphyry copper systems; Economic Geology, v. 105, p. 3–41.

Simmons, S.F., White, N.C. and John, D. (2005): Geological characteristics of epithermal precious and base metal deposits; *in* Economic Geology One Hundreth Anniversary Volume 1905–2005, J.W. Hedenquist, J.F.H. Thompson, R.J. Goldfarb and J.P. Richards (ed.), Economic Geology, p. 485–522.

Spectral Evolution (2019): SpecMIN™: reference mineral spectral library; Spectral International, Inc., URL <https://spectralevolution.com/products/software/mining-software/> [November 2019].

SRK Consulting Inc. (2016): Technical report for the Kemess underground project and Kemess East resource estimate, British Columbia, Canada; prepared for AuRico Metals Inc., 409 p., URL <https://www.centerragold.com/cg-raw/cg/KemessUG_Updated_Technical-Report_2CA046-004_20160506_FNL.pdf> [May 2019].

Stoffregen, R.E. (1987): Genesis of acid-sulfate alteration and Au-Cu-Ag mineralization at Summitville, Colorado; Economic Geology, v. 82, p. 1575–1591.

van Straaten, B.I. and Bouzari, F. (2018): The Middle Jurassic Tanzilla-McBride hydrothermal system: one of the largest lithocaps in BC?; Mineral Exploration RoundUp, Vancouver, BC, January 22–25, 2018, poster presentation.

van Straaten, B.I. and Gibson, R. (2017): Late Early to Middle Jurassic Hazelton Group volcanism and mineral occurrences in the McBride-Tanzilla area, northwest British Columbia; *in* Geological Fieldwork 2016, BC Ministry of Energy, Mines and Petroleum Resources, BC Geological Survey, Paper 2017-1, p. 83–115, URL <http://cmscontent.nrs.gov.bc.ca/geoscience/PublicationCatalogue/Paper/BCGS_P2017-01-06_vanStraaten.pdf> [May 2019].

van Straaten, B.I. and Nelson, J.L. (2016): Syncollisional late Early to early Late Jurassic volcanism, plutonism, and porphyry-style alteration on the northeastern margin of Stikinia; *in* Geological Fieldwork 2015, BC Ministry of Energy, Mines and Petroleum Resources, BC Geological Survey, Paper 2016–1, p. 113–143, URL <http://cmscontent.nrs.gov.bc.ca/geoscience/PublicationCatalogue/Paper/BCGS_P2016-01-07_vanStraaten.pdf> [May 2019].

van Straaten, B.I., Gibson, R. and Nelson, J. (2017): Preliminary bedrock geology of the Tanzilla and McBride area, British Columbia; BC Ministry of Energy, Mines and Petroleum Resources, BC Geological Survey, Open File 2017-9, scale 1:50 000, URL <http://cmscontent.nrs.gov.bc.ca/geoscience/PublicationCatalogue/OpenFile/BCGS_OF2017-09.pdf> [May 2019].